

<b>3</b>	<b>SCIENCE CASE FOR THE NOvA EXPERIMENT.</b>	<b>3-1</b>
3.1	OVERVIEW OF NEUTRINO OSCILLATIONS	3-1
3.2	DETAILS OF NEUTRINO OSCILLATIONS	3-2
3.2.1	<i>Neutrino Mixing</i>	3-2
3.2.2	<i>Present Knowledge of the Mixing Parameters</i>	3-2
3.2.3	<i>Matter Effects</i>	3-4
3.2.4	<i>Ambiguities</i>	3-5
3.3	NOvA CAPABILITIES IN $\nu_\mu \rightarrow \nu_e$ OSCILLATION MEASUREMENTS	3-6
3.3.1	<i>Sensitivity to <math>\sin^2(2\theta_{13})</math></i>	3-6
3.3.2	<i>Sensitivity to the Mass Ordering</i>	3-7
3.4	MEASUREMENT OF THE DOMINANT MODE OSCILLATION PARAMETERS VIA $\nu_\mu$ DISAPPEARANCE.	3-10
3.5	MEASUREMENT OF THE SIGN OF $\cos(2\theta_{23})$	3-12
3.6	SEARCH FOR “ATMOSPHERIC” STERILE NEUTRINOS	3-13
3.7	CHAPTER 3 REFERENCES	3-14

## 3 Science Case for the NOvA Experiment.

### 3.1 Overview of Neutrino Oscillations

The standard picture of neutrinos consists of three different types:  $\nu_e$ ,  $\nu_\mu$ , and  $\nu_\tau$ , each of which is a partner to a charged lepton:  $e$  (electron),  $\mu$  (muon), and  $\tau$  (tau lepton). We know that the neutrinos have mass and as a result, one type of neutrino can transform (oscillate) into another type. Oscillations of  $\nu_e$  into  $\nu_\mu + \nu_\tau$  have been observed in solar neutrino experiments [1] and in a long baseline reactor neutrino experiment [2] with an oscillation length of approximately 15,000 km/GeV. Oscillations of  $\nu_\mu$  into  $\nu_\tau$  have been observed in atmospheric neutrino experiments [3], in a Japanese accelerator experiment [4], and in the MINOS experiment now running in the Fermilab NuMI beam [5] with an oscillation length of approximately 500 km/GeV, known as the “atmospheric oscillation length.” Oscillations between  $\nu_\mu$  and  $\nu_e$  have yet to be observed at the atmospheric oscillation length. There is an upper limit on the rate of this oscillation from a reactor neutrino experiment [6]. The primary goal of the NOvA experiment is to observe and study  $\nu_\mu \rightarrow \nu_e$  oscillations at the atmospheric oscillation length.

The rate of the  $\nu_\mu \rightarrow \nu_e$  oscillation is expressed mathematically in terms of a mixing angle,  $\theta_{13}$ , and the number of signal events observed in the oscillation is roughly proportional to  $\sin^2(2\theta_{13})$ . For neutrino beams that pass through the earth, the rate of the  $\nu_\mu \rightarrow \nu_e$  oscillation also depends on the ordering of the masses of the three species of neutrinos. If the two neutrinos that cause the solar oscillations have lower masses than the third neutrino, called the “normal mass ordering,” then neutrino oscillations are enhanced and antineutrino oscillations are attenuated. If the mass ordering is reversed, call “inverted mass ordering,” then the antineutrino oscillations are enhanced and the neutrino oscillations are attenuated. Currently, we have no information on the mass ordering. Additionally, the rate of  $\nu_\mu \rightarrow \nu_e$  oscillations depends on a phase angle that violates charge-parity (CP) symmetry. A non-zero value of this phase angle,  $\delta$ , leads to CP violation in the lepton sector and may have a bearing on the origin of the matter-antimatter asymmetry of the universe.

The goal of the NOvA experiment is to extend the search for  $\nu_\mu \rightarrow \nu_e$  oscillations by roughly an order of magnitude beyond the sensitivity of the MINOS experiment. Additionally,

NOvA can begin to study the mass ordering and search for the effects of the CP violating phase angle  $\delta$ . NOvA is particularly well suited to the study of the mass ordering due to the large amount of earth between the neutrino source and the detector. No other planned experiment can attack this problem.

This chapter outlines the neutrino oscillation formalism in more mathematical detail and describes the reach of NOvA for this physics.

## 3.2 Details of Neutrino Oscillations

### 3.2.1 Neutrino Mixing

Neutrino oscillations come about because the weak eigenstates are rotated from the mass eigenstates. The unitary matrix that rotates the mass eigenstates into flavor eigenstates is

$$\begin{pmatrix} \nu_e \\ \nu_\mu \\ \nu_\tau \end{pmatrix} = \begin{pmatrix} c_{13}c_{12} & c_{13}s_{12} & s_{13}e^{-i\delta} \\ -c_{23}s_{12} - s_{13}s_{23}c_{12}e^{i\delta} & c_{23}c_{12} - s_{13}s_{23}s_{12}e^{i\delta} & c_{13}s_{23} \\ s_{23}s_{12} - s_{13}c_{23}c_{12}e^{i\delta} & -s_{23}c_{12} - s_{13}c_{23}s_{12}e^{i\delta} & c_{13}c_{23} \end{pmatrix} \begin{pmatrix} \nu_1 \\ \nu_2 \\ \nu_3 \end{pmatrix}, \quad (3.1)$$

where  $c_{jk} \equiv \cos\theta_{jk}$  and  $s_{jk} \equiv \sin\theta_{jk}$ . With this labeling, the atmospheric neutrino oscillations are primarily determined by the  $\theta_{23}$  and  $\Delta m_{32}^2$  parameters, whereas the solar neutrino oscillations depend on  $\theta_{12}$  and  $\Delta m_{12}^2$ , where  $\Delta m_{ij}^2 = m_i^2 - m_j^2$ . If the phase  $\delta$  is neither 0 nor  $\pi$ , then neutrinos exhibit CP violation.

### 3.2.2 Present Knowledge of the Mixing Parameters

The SuperKamiokande[7], KEK[4], and MINOS[5] experiments have all measured the atmospheric oscillation parameters  $|\Delta m_{atm}^2| \approx |\Delta m_{31}^2| \approx |\Delta m_{32}^2|$  and  $\sin^2 2\theta_{23}$ . The results are summarized in Fig. 3.1. The combined analysis[2] of the SNO[2], SuperKamiokande[4] and KamLAND[3] experiments give  $\Delta m_{21}^2 = +7.9 \pm 0.6 \times 10^{-5} \text{ eV}^2$  and  $\sin^2 2\theta_{12} = 0.82 \pm 0.07$  for the solar parameters. The CHOOZ experiment [6] provides a limit of  $\sin^2 2\theta_{13} < 0.15$  for  $\Delta m_{32}^2 = 0.0024 \text{ eV}^2$ , the central value of the MINOS measurement.

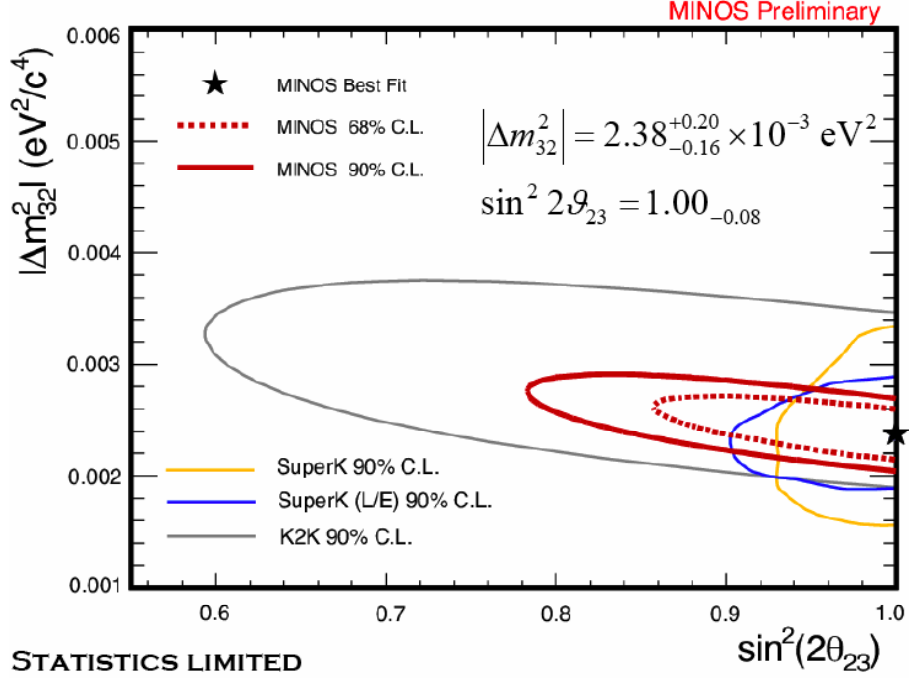


Fig. 3.1 Confidence intervals from the SuperKamiokande[7], K2K[4], and MINOS[5] experiments. The plot is from Ref. 5.

### 3.2.3 $\nu_e$ Appearance Probability

The appearance probability of  $\nu_e$  in a  $\nu_\mu$  beam in vacuum is given by the sum of three terms,

$$P_{vac}(\nu_\mu \rightarrow \nu_e) = P_{atm} + P_{sol} + P_{int}. \quad (3.2)$$

$P_{atm}$  represents the oscillation governed by the atmospheric oscillation length,

$$P_{atm} = \sin^2 \theta_{23} \sin^2 2\theta_{13} \sin^2 \Delta_{31}, \quad (3.3)$$

where

$$\Delta_{ij} \approx 1.27 \left( \frac{\Delta m_{ij}^2 L}{E} \right) \quad (3.4)$$

where  $\Delta m_{31}^2$  is measured in  $\text{eV}^2$ ,  $L$  is measured in km, and  $E$  is measured in GeV.  $P_{sol}$  represents the oscillation governed by the solar oscillation length,

$$P_{sol} = \cos^2 \theta_{13} \cos^2 \theta_{23} \sin^2 2\theta_{12} \sin^2 \Delta_{21}. \quad (3.5)$$

And  $P_{int}$  represents the interference between the solar and atmospheric oscillation lengths. It has both a CP conserving and CP violating term,

$$P_{int} = J [\cos \delta \cos \Delta_{32} \sin \Delta_{31} \sin \Delta_{21} \pm \sin \delta \sin \Delta_{32} \sin \Delta_{31} \sin \Delta_{21}], \quad (3.6)$$

where

$$J = \cos \theta_{13} \sin \theta_{12} \sin \theta_{13} \sin \theta_{23}, \quad (3.7)$$

and the top sign in the CP violating term refers to neutrinos and the bottom sign to antineutrinos.

While the solar term,  $P_{sol}$ , is insignificant for the NO $\nu$ A, the interference term,  $P_{int}$ , is

comparable to the atmospheric term. Further, since  $P_{int}$  is first order in the small parameter  $\theta_{13}$

while  $P_{atm}$  is second order in  $\theta_{13}$ , the significance of the CP-violating asymmetry between

neutrino and antineutrino oscillations is roughly independent of  $\theta_{13}$ .

### 3.2.3 Matter Effects

The neutrinos in the NuMI beam propagate through the earth and a coherent charged-current forward scattering of electron-type neutrinos with electrons in the earth induces a significant change in the oscillation probabilities. These matter effects have opposite sign for neutrinos and antineutrinos and for the normal versus inverted neutrino mass orderings. The matter effects can thus be used to distinguish the two possible three-neutrino mass orderings shown in Figure 3.2.

The matter effects modify  $\sin \Delta_{21}$  and  $\sin \Delta_{31}$  in Eqs. 3.3, 3.5, and 3.6 by the substitution

$$\sin \Delta_{ij} \rightarrow \frac{\Delta_{ij}}{\Delta_{ij} \pm aL} \sin(\Delta_{ij} \pm aL) \quad (3.8)$$

where the top sign refers to neutrinos and the bottom sign to antineutrinos and

$$a = \frac{G_F \rho_e}{\sqrt{2}} \approx (3700 \text{ km})^{-1} \left( \frac{\rho}{2.8 \text{ g cm}^{-3}} \right), \quad (3.9)$$

where  $\rho_e$  is the electron density in the earth and  $\rho$  is the density of the earth. If the experiment is performed at the first oscillation peak, the matter effects are primarily a function of the energy of the neutrino beam and the transition probability in matter can be approximated by

$$P_{mat}(\nu_\mu \rightarrow \nu_e) \approx \left( 1 \pm \frac{E}{6 \text{ GeV}} \right) P_{vac}(\nu_\mu \rightarrow \nu_e). \quad (3.10)$$

For the normal hierarchy, matter effects enhance (suppress) the transition probability for neutrinos (antineutrinos) and vice versa for the inverted hierarchy. For the NOvA experiment, matter effects give approximately a 30% enhancement or suppression in the transition probability.

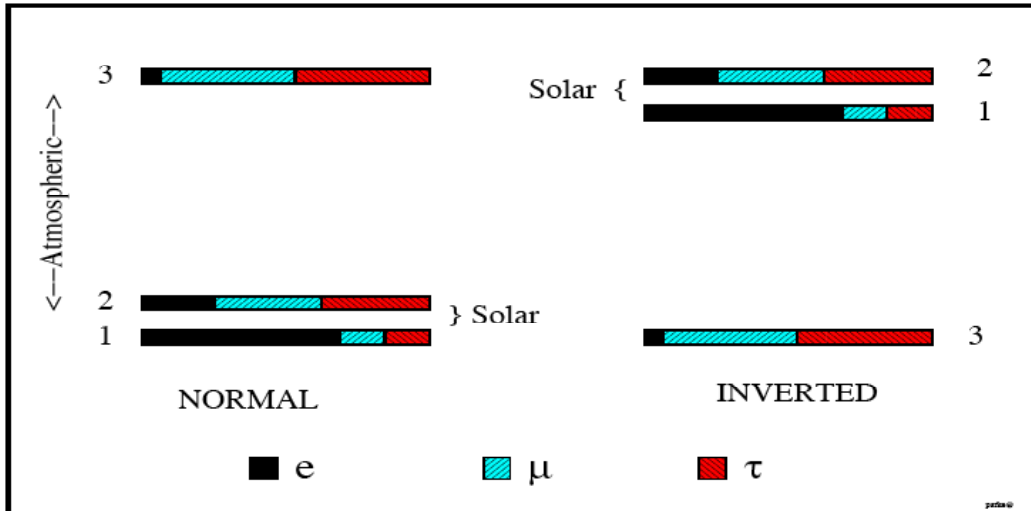


Fig. 3.2 The two allowed three-neutrino mass squared spectra that account for the oscillations of solar and atmospheric neutrinos. The normal spectrum has  $\Delta m_{32}^2 > 0$  and the inverted spectrum has  $\Delta m_{32}^2 < 0$ . The  $\nu_e$  fraction of each mass eigenstate is indicated by the black solid region, whereas the  $\nu_\mu$  ( $\nu_\tau$ ) fraction is indicated by the blue-green right-leaning (red left-leaning) hatching. The  $\nu_e$  fraction in the mass eigenstate labeled 3 has been enhanced for clarity.

### 3.2.4 Ambiguities

Since the matter effect is caused by the interaction of electron-type neutrinos with electrons in the earth, it has the opposite sign for neutrinos and antineutrinos and can be confused with a true CP-violating effect. This leads in some cases to an inherent ambiguity between the CP phase  $\delta$  and the mass ordering.

Figure 3.3 shows an illustration of this ambiguity. It illustrates the parameters consistent with a NOvA measurement of a 2%  $\nu_\mu \rightarrow \nu_e$  oscillation probability for  $|\Delta m_{atm}^2| = 0.0024 \text{ eV}^2$ .

Possible values of  $\sin^2(2\theta_{13})$  are shown on the vertical axis, the CP-violating phase  $\delta$  is shown by the ellipses, and the two mass orderings are shown by the two ellipses. The result of a  $\bar{\nu}_\mu \rightarrow \bar{\nu}_e$  oscillation measurement is shown on the horizontal axis. If the signs of the CP violation effect and the matter effect are the same, for example  $\delta$  near  $3\pi/2$  for the normal mass ordering or  $\delta$  near  $\pi/2$  for the inverted mass ordering, then there is no ambiguity and NOvA can determine the mass ordering. However, if  $\delta$  is such that the ellipses overlap, then there is an inherent ambiguity can only be resolved by a third measurement, either at a different baseline, such as will be done by the T2K experiment, or by a measurement a different point in the dynamic phase, such as at the second oscillation maximum.

Since the relative size of the asymmetry due to CP violation increases as  $\sin^2(2\theta_{13})$  decreases and the relative size of the matter effect stays constant, the fraction of possible  $\delta$  values for which there is an ambiguity increases with decreasing values of  $\theta_{13}$ .

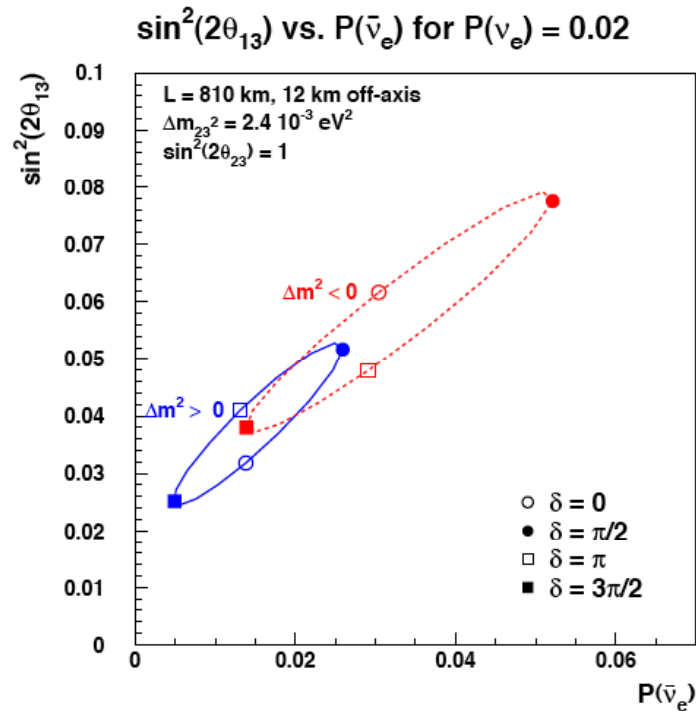


Fig. 3.3: Plot of the possible results for  $\sin^2(2\theta_{13})$  vs. the oscillation probability observed for antineutrinos given a perfectly measured 2% neutrino oscillation probability. The solid (blue) curve is for the normal mass ordering, and the dashed (red) curve is for the inverted mass ordering. The values of the CP-violating phase  $\delta$  are indicated in each case by the open and closed circles and squares with the key on the figure.

### 3.3 NOvA Capabilities in $\nu_\mu \rightarrow \nu_e$ Oscillation Measurements

NOvA plans to split its running time equally between with the horns focusing positive particles (neutrino running) and negative particles (antineutrino running). Even though the rates are higher for neutrino running than antineutrino running, there are two reasons for this strategy. First, it makes the sensitivity to seeing a signal less dependent on the value of  $\delta$  and the sign of  $\Delta m_{am}^2$ . Second, without antineutrino running, NOvA would have no ability to measure  $\delta$  or the sign of  $\Delta m_{am}^2$ .

In the following, we will show the capabilities of the NOvA experiment assuming a 15 kT detector with both  $36 \times 10^{20}$ ,  $60 \times 10^{20}$ , and  $120 \times 10^{20}$  protons on target (pot). The first corresponds to 6 full years (44 weeks per year) of running at 700 kW beam power, assuming the NuMI and accelerator upgrades included in the NOvA project as discussed in Chapter 2 and Chapter 8. The last two corresponds to 6 full years of running at 1.2 MW and 2.3 MW beam power with the conceptual SNuMI and Project X upgrades, also discussed in Chapter 2, Sections 2.3 and 2.4. These latter beam powers are included to illustrate the potential of the NOvA experiment if either of these projects were to be accomplished. The sensitivity calculations have been done using the results of the simulations discussed in Chapter 6 assuming a systematic uncertainty in the background extrapolation from the near to far detector of 10%. These calculations take into account the antineutrinos in the neutrino running (1.5%) and the neutrinos in the antineutrino running (3.8%).

#### 3.3.1 Sensitivity to $\sin^2(2\theta_{13})$

Figure 3.4 shows the sensitivity to  $\theta_{13} \neq 0$  at the three standard deviation level as a function of  $\delta$  for each of the mass orderings. A way of comparing the difference between 700 kW, 1.2 MW, and 2.3 MW beam power is to note the fraction of the parameter space for which the NOvA three-standard deviation sensitivity is more than an order of magnitude greater than the Chooz experiment 90% upper limit. The 2.3 MW and 1.2 MW sensitivities meet this criterion for 64% and 22% of the parameter space, respectively, while the 700 kW sensitivities meet it for only 9.5% of the parameter space.

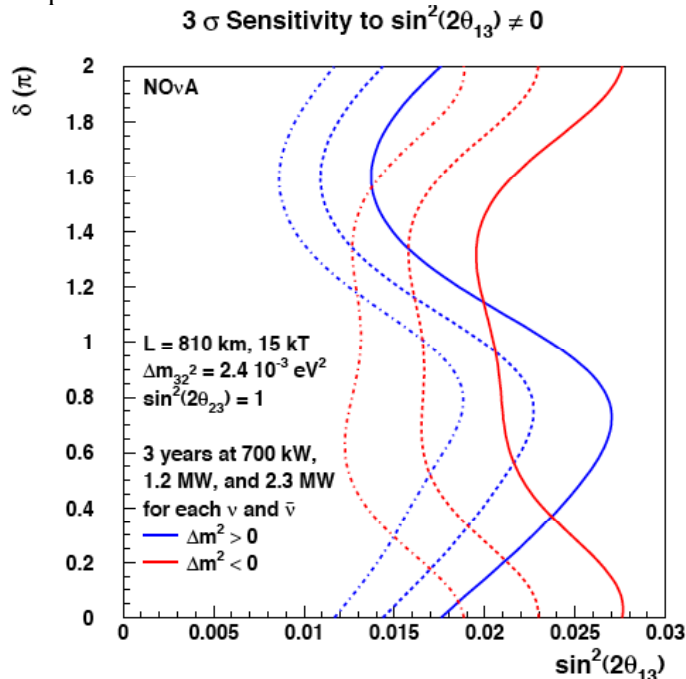


Fig. 3.4: Three standard deviation sensitivity to  $\theta_{13} \neq 0$  as a function of the CP-violating phase  $\delta$  for a 6-years of NOvA running split evenly between neutrino and antineutrino running. The solid curves are for 700 kW beam power, the dashed curves are for 1.2 MW beam power, and the dot-dashed curves are for 2.3 MW beam power. The blue (more S-shaped) curves are for the normal mass ordering and the red curves are for the inverted mass ordering.

### 3.3.2 Sensitivity to the Mass Ordering

Figure 3.5 shows the sensitivity to the mass ordering at the 95% confidence level as a function of  $\delta$  for each of the mass orderings. The dot-dashed and dashed lines show the sensitivity for 2.3 MW and 1.2 MW running, respectively, and the solid lines show the sensitivity for 700 kW running. As explained above, the mass ordering can only be resolved by NOvA alone for the portion of the parameter space in which the matter effect and CP violation affect the oscillation in the same manner. For the remainder of the parameter space, a third measurement is required to resolve the mass ordering. One possibility is to combine NOvA data with data from T2K, which has a much shorter baseline. Figure 3.6 shows the effect of combining NOvA results with those from a 6-year neutrino run from the T2K experiment. It is assumed that the T2K beam power will upgrade in a similar way to the possible NOvA beam upgrades.[8]

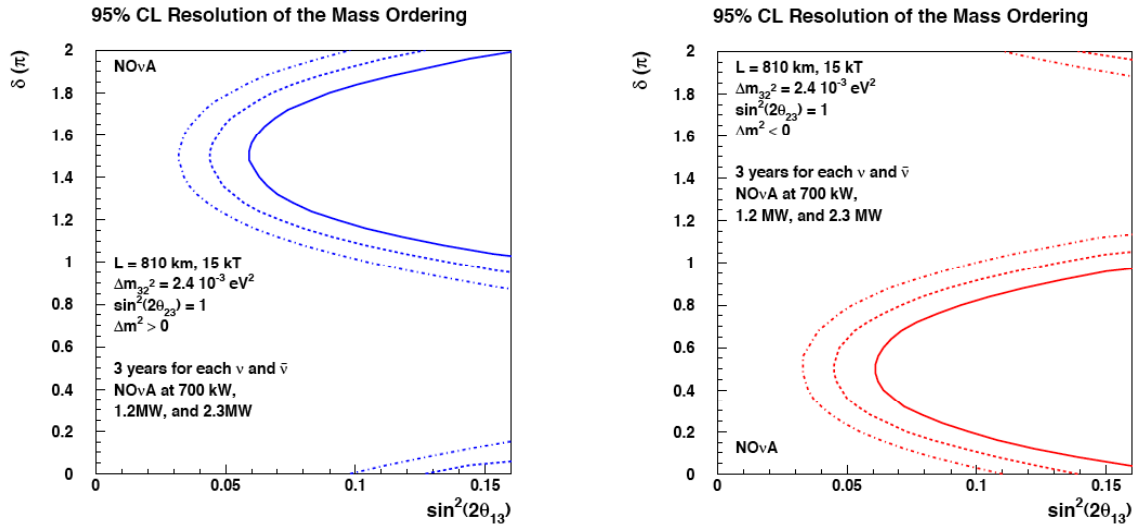


Fig. 3.5: 95% resolution of the mass ordering as a function of the CP-violating phase  $\delta$  for 6-years of NOvA running split evenly between neutrino and antineutrino running. The dot-dashed and dashed curves are for 2.3 MW and 1.2 MW beam power, respectively, and the solid curves are for 700 kW beam power. The left graph is for the normal mass ordering and the right graph is for the inverted mass ordering.

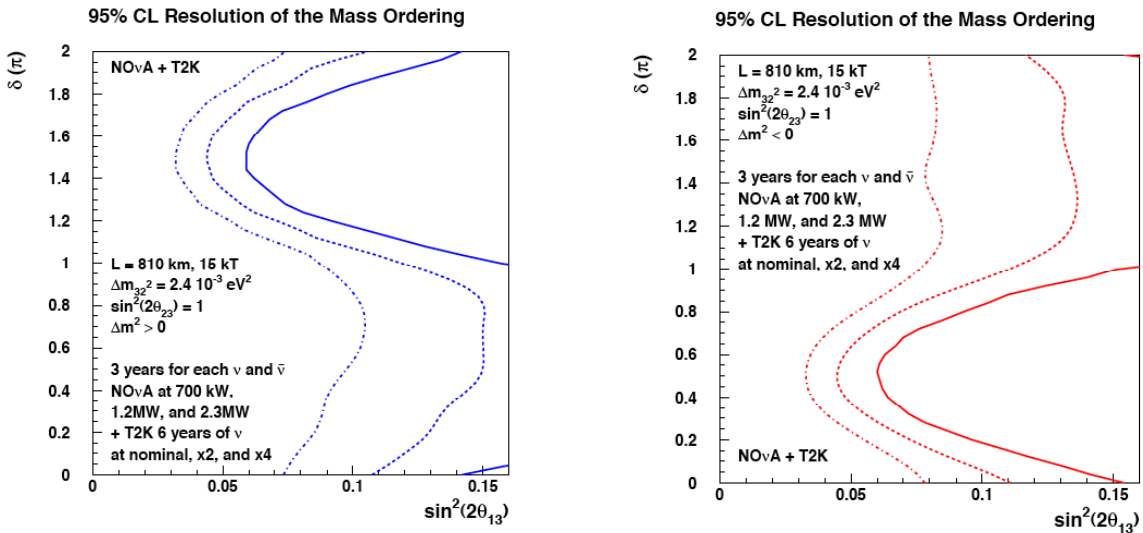


Fig. 3.6: 95% resolution of the mass ordering as a function of the CP-violating phase  $\delta$  for 6 years of NOvA running split evenly between neutrino and antineutrino running combined with 6 years of T2K running on neutrinos. The dot-dashed and dashed curves are for 2.3 MW and 1.2 MW beam power, respectively, and the solid curves are for 700 kW beam power for NOvA. It is assumed that T2K will upgrade its beam power in parallel with NOvA. Thus, the 1.2 MW NOvA plot is paired with twice nominal T2K power and 2.3 MW NOvA plot is paired with four times nominal T2K power. The left graph is for the normal mass ordering and the right graph is for the inverted mass ordering.

### 3.3.3 Sensitivity to the CP-Violating Phase $\delta$

Figures 3.7 and 3.8 show contours in the  $\sin^2(2\theta_{13})$  -  $\delta$  plane for a sample point,  $\sin^2(2\theta_{13}) = 0.06$  and  $\delta = 3\pi/2$ . Figure 3.7 shows the one standard deviation contour for 2.3 MW, 1.2 MW and 700 kW running. Figure 3.8 shows the one, two, and three standard deviation contours for 2.3 MW running. There is not enough statistical power to demonstrate CP-violation at three standard deviation level, but there is enough sensitivity to give an indication of the type of future experiments that will be necessary. For cases in which the mass ordering is not determined, there will also be contours for the alternative mass ordering hypothesis.

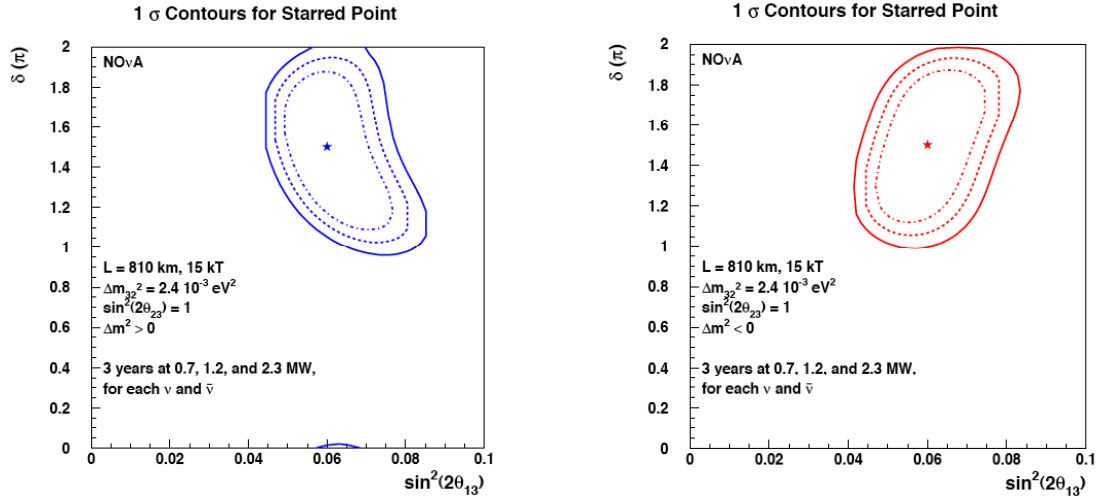


Fig. 3.7: Expected 1-standard deviation contour for a sample point,  $\sin^2(2\theta_{13}) = 0.06$ ,  $\delta = 3\pi/2$ , for 6-years of NOvA running split evenly between neutrino and antineutrino running. The solid contour is for 0.7 MW beam power, the dashed contour is for 1.2 MW beam power, and the dot-dashed curve is for 2.3 MW beam power. The left graph is for the normal beam ordering and the right graph is for the inverted mass ordering.

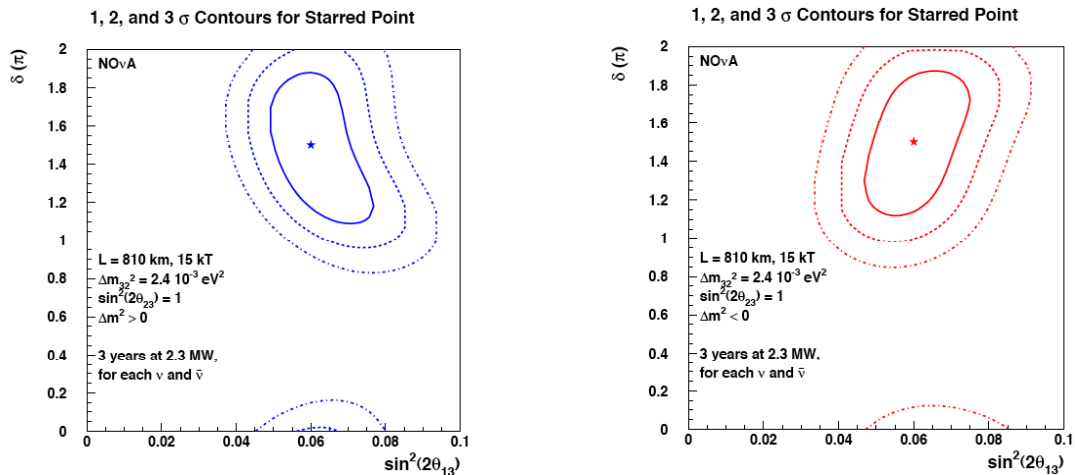


Fig. 3.8: Expected 1, 2, and 3-standard deviation contours for the sample point and conditions of Fig. 3.7 for 2.3 MW beam power.

### 3.4 Measurement of the Dominant Mode Oscillation Parameters Via $\nu_\mu$ Disappearance.

Although the primary NOvA physics goal is the study of  $\nu_\mu \rightarrow \nu_e$  oscillations, NOvA will also be able to make significant measurements of the dominant mode oscillation parameters,  $\sin^2(2\theta_{23})$  and  $\Delta m_{32}^2$ . The best current measurement of  $\sin^2(2\theta_{23})$  comes from the SuperKamiokande study of atmospherically produced neutrinos [7] and is shown in Fig. 3.1. This measurement is consistent with maximal mixing,  $\sin^2(2\theta_{23}) = 1$ , but with a considerable uncertainty. At the 90% confidence level,  $\sin^2(2\theta_{23}) > 0.92$ , which translates into a rather large range of possible values of  $\sin^2 \theta_{23}$ , namely  $0.36 < \sin^2 \theta_{23} < 0.64$ .

There are three reasons why determining  $\sin^2(2\theta_{23})$  is of high interest:

- (1) If the mixing is maximal, it might be due to some currently unknown symmetry.
- (2) The  $\nu_\mu \rightarrow \nu_e$  oscillation is mostly proportional to  $\sin^2(\theta_{23})\sin^2(2\theta_{13})$  while  $\bar{\nu}_e$  disappearance, measured by reactor experiments, is proportional to  $\sin^2(2\theta_{13})$ . Thus, if the mixing is not maximal, there is an ambiguity in comparing accelerator and reactor experiments.
- (3) Conversely, whether  $\theta_{23}$  is greater than or less than  $\pi/4$ , which measures whether the third neutrino mass eigenstate couples more strongly to  $\nu_\mu$ 's or  $\nu_\tau$ 's, can best be measured by comparing precise accelerator and reactor measurements. (See Section 3.5.)

The deviation of  $\sin^2(2\theta_{23})$  from unity is measured by the depth of the oscillation dip in the  $\nu_\mu$  disappearance spectrum. Thus, precision in this quantity requires good statistics in this region, excellent neutrino energy resolution, and good control of systematics. NOvA offers the possibility of satisfying all of these requirements.

It appears that the best way to meet these requirements is to limit the analysis to totally contained quasielastic events, i.e., those events in which the geometrical pattern of energy deposition is consistent with the presence of only an energetic muon and a possible recoil proton. We have performed a preliminary study of how well NOvA can use these events to measure  $\sin^2(2\theta_{23})$  and  $\Delta m_{32}^2$  using a parametric representation of the energy. This procedure is justified by the nature of these events, which are extremely clean.

The calculated one and two standard deviation contours are displayed in Figure 3.9 for assumed values of  $\sin^2(2\theta_{23})$  of 0.95, 0.98, and 1.00 and a six-year run equally divided between neutrinos and antineutrinos for beam powers of 700 kW, 1.2 MW, and 2.3 MW. The energy resolution has been assumed to be 2%, but the contours do not change markedly as one increases the resolution to 4%.

Note that the precision of the  $\sin^2(2\theta_{23})$  measurement increases as the value of  $\sin^2(2\theta_{23})$  approaches unity. For maximal mixing, the error on the measurement of  $\sin^2(2\theta_{23})$  is about 0.003 for 700 kW power and somewhat smaller for the other beam powers.

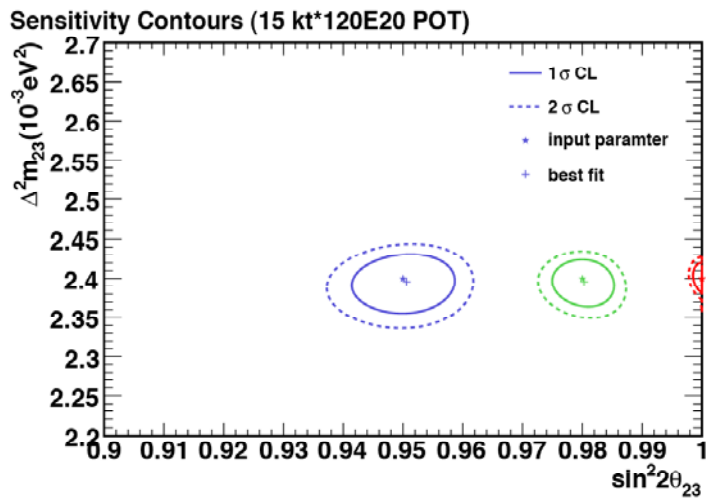
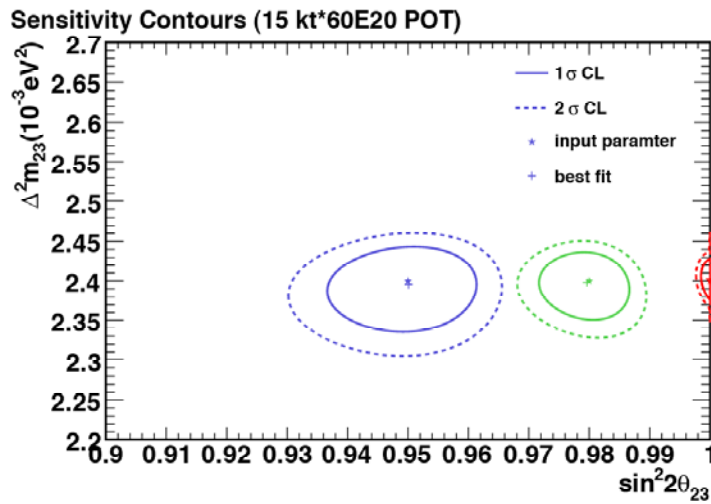
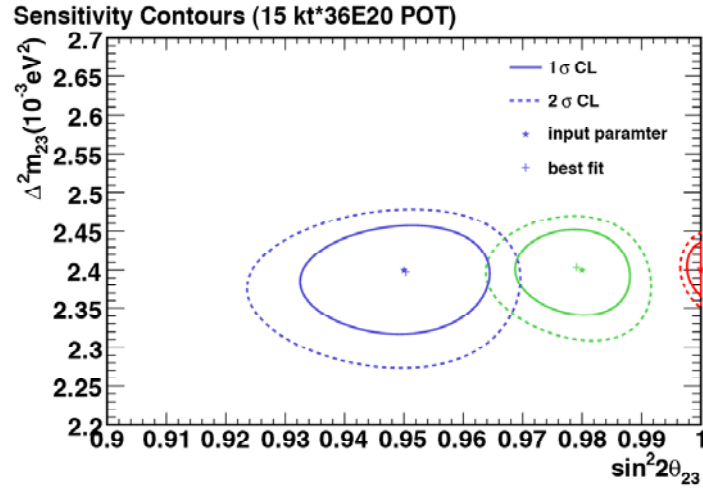


Fig. 3.9: One and two standard deviation contours for a simultaneous measurement of  $\Delta m_{32}^2$  and  $\sin^2(2\theta_{23})$  for a six-year run at equally divided between neutrinos and antineutrinos. The three input values are indicated by a star and the best fit for each is indicated by a plus sign. The top plot is for 700 kW beam power, the middle for 1.2 MW, and the bottom for 2.3 MW.

### 3.5 Measurement of the Sign of $\cos(2\theta_{23})$

As mentioned in the previous section, if the dominant atmospheric oscillation is not maximal, it is interesting to determine whether  $\theta_{23}$  is greater than or less than  $\pi/4$ , which measures whether  $\nu_e$ 's oscillate more strongly to  $\nu_\mu$ 's or  $\nu_\tau$ 's. This can be done most easily by comparing the results of the NOvA experiment with a reactor experiment, such as Daya Bay[9], since a reactor experiment will measure the oscillation of  $\bar{\nu}_e$ 's into the sum of  $\bar{\nu}_\mu$ 's and  $\bar{\nu}_\tau$ 's while an accelerator experiment will measure the oscillation of  $\nu_\mu$ 's into  $\nu_e$ 's.

Figure 3.10 shows the region of  $\sin^2(2\theta_{23}) - \sin^2(2\theta_{13})$  parameter space for which this measurement can be made at the 95% confidence level assuming that a reactor experiment can reach a one standard deviation precision of 0.005. The limits are functions of the CP-violating phase  $\delta$ , the mass ordering, and the sign of  $\cos(2\theta_{23})$ ; the values in Fig. 3.10 are averages over the parameter space.

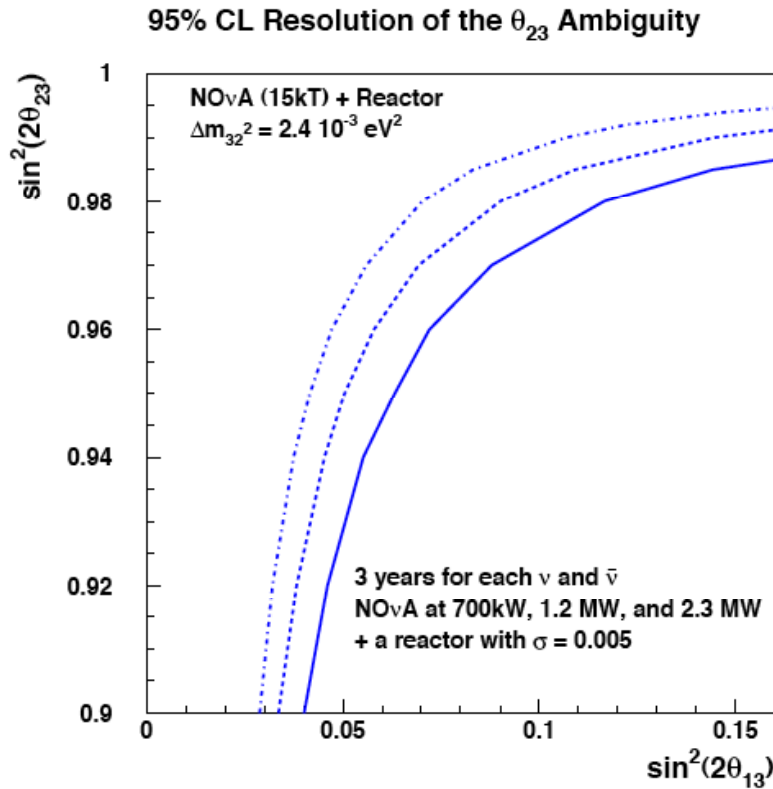


Fig. 3.10: The  $\sin^2(2\theta_{23}) - \sin^2(2\theta_{13})$  regions to the right of the curves are those in which the sign of  $\cos(2\theta_{23})$  can be resolved at the 95% confidence level by a comparison of data from NOvA and a reactor experiment that can achieve a one standard deviation sensitivity of 0.005 in  $\sin^2(2\theta_{13})$ . The solid curve represents a 6-year NOvA run divided equally between neutrino and antineutrino running at 700 kW beam power and the dotted and dash-dotted curves represents the same run at 1.2 MW and 2.3 MW beam power, respectively. The regions are somewhat sensitive to  $\delta$ , the mass ordering, and the sign of  $\cos(2\theta_{23})$ ; the curves represent an average over the parameter space.

### 3.6 Search for “atmospheric” sterile neutrinos

The Super-Kamiokande, K2K, and MINOS experiments each study neutrino oscillations via muon neutrino disappearance. Of these experiments, only Super-Kamiokande has any indications that the oscillations are in fact due to  $\tau$  neutrinos, [10] leaving open the possibility that oscillations at the atmospheric scale could involve a fourth light neutrino. To be consistent with LEP measurements of  $Z^0$  decays, this fourth neutrino state would have to be sterile, that is, to have zero coupling to the Z and W bosons. Super-Kamiokande has ruled out the possibility that oscillations at the atmospheric scale could be entirely due to oscillations to sterile neutrinos [11]. Allowing for the possibility that muon neutrinos oscillate to a neutrino state which is an admixture of  $\nu_\tau$  and  $\nu_s$ , Super-Kamiokande limits the sterile content to below 23% at the 90% confidence level [12].

In NOvA, participation of a sterile neutrino state in the oscillations of muon neutrinos would suppress the neutral-current event rate as measured at the far detector. Based on detailed simulations, the NOvA detector can select a neutral-current (NC) event sample of 91% purity with an efficiency for retaining neutral-current events with 56% efficiency. Figure 3.11 shows the resulting visible energy spectrum for the reconstructed NC sample. As seen in the Figure 3.11, increasing the sterile admixture only affects the spectrum significantly below 2 GeV in visible energy. The ratio of the number of NC events below 2 GeV to those above 2 GeV provides a measure of the sterile admixture. In this ratio, we expect systematic uncertainties in the detection efficiency, neutrino cross-sections, and neutrino flux to largely cancel, leaving a 5% systematic uncertainty on the sterile admixture. In this way, NOvA can limit the sterile admixture to below 11% at 90% C.L., an improvement of slightly more than a factor of two on the limit from Super-Kamiokande.

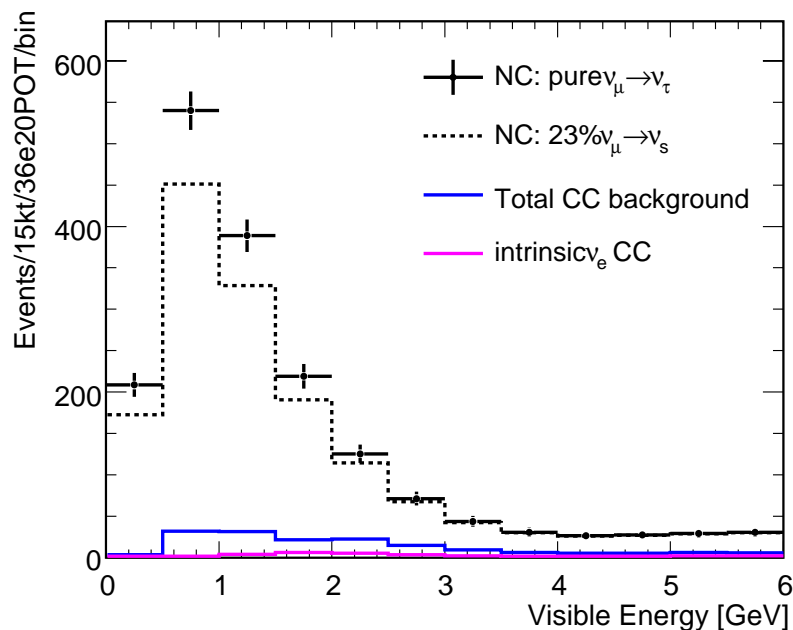


Fig. 3.11: The visible energy spectrum of neutral-current events reconstructed in the NOvA detector. Points show the expected spectrum for oscillations to a pure tau neutrino state, while the dotted curve shows the expectation for a sterile admixture at the current Super-Kamiokande limit. The blue and red curves show the background from charged-current muon and electron neutrino events in the neutral-current sample.

### 3.7 Chapter 3 References

- [1] Q. R. Ahmad et al. [SNO Collaboration], *Phys. Rev. Lett.* **87**, 071301 (2001); S.N. Ahmed et al. *Phys.Rev.Lett.* **92**, 181301 (2004).
- [2] K. Eguchi et al. [KamLAND Collaboration], *Phys. Rev. Lett.* **90**, 021802 (2003); T. Araki et al., *Phys.Rev.Lett.* **94**, 081801 (2005).
- [3] S. Fukuda et al. [Super-Kamiokande Collaboration], *Phys. Lett.* **B539**, 179 (2002).
- [4] M. H. Ahn et al. [K2K Collaboration], *Phys. Lett.* **B511**, 178 (2001); *Phys. Rev. Lett.* **90**, 041801 (2003); E. Aliu et al., hep-ex/0411038 (2004).
- [5] D. G. Michael et al. [MINOS Collaboration], *Phys.Rev.Lett.* **97**, 191801 (2006); J. Thomas, "Accelerator Neutrino Experiments," to appear in the proceedings of the XXIII International Symposium on Lepton and Photon Interactions at High Energy, August 13-18, 2007, Daegu, Korea, ([http://chep.knu.ac.kr/lp07/htm/s11\\_01\\_01.htm](http://chep.knu.ac.kr/lp07/htm/s11_01_01.htm)).
- [6] CHOOZ collaboration, M. Apollonio *et al.*, *Phys. Lett. B* **466** (1999) 415; *Eur. Phys. J. C* **27** (2003) 331
- [7] Y. Ashie et al. . [Super-Kamiokande Collaboration], *Phys. Rev. Lett.* **93**, 101801 (2004); *Phys. Rev. D* **71**, 112005 (2005).
- [8] M. Zito, "The T2K neutrino oscillation experiment," to appear in the proceedings of the 2007 Europhysics Conference on High Energy Physics, July 19-25, 2007, Manchester, England, (<http://www.hep.man.ac.uk/HEP2007/index.html>).
- [9] Daya Bay Proposal, hep-ex/0701029v1 (2007).
- [10] K. Abe et al., *Phys.Rev.Lett.***97**:171801,2006
- [11] S. Fukuda et al., *Phys. Rev. Lett.* **85**, 3999 - 4003 (2000)
- [12] W. Wang, Ph.D. Thesis, Boston University (2007).